Modeling and Box-Behnken design optimization of photocatalytic parameters for efficient removal of dye by lanthanum-doped mesoporous TiO2

Hanane Chaker, Nawal Ameur, Karima Saidi-Bendahou, Mustapha Djennas, Sophie Fourmentin

To cite this version:

Hanane Chaker, Nawal Ameur, Karima Saidi-Bendahou, Mustapha Djennas, Sophie Fourmentin. Modeling and Box-Behnken design optimization of photocatalytic parameters for efficient removal of dye by lanthanum-doped mesoporous TiO2. Journal of Environmental Chemical Engineering, 2021, 9 (1), pp.104584. 10.1016/j.jece.2020.104584 . hal-04242280

HAL Id: hal-04242280
https://hal.science/hal-04242280v1

Submitted on 22 Jul 2024

Modeling and Box-Behnken design optimization of photocatalytic parameters for efficient removal of dye by lanthanum-doped mesoporous TiO_2

Hanane Chaker[*a,b, c], **Nawal Ameur** [a,d], **Karima Saidi-Bendahou** [a], **Mustapha Djennas** [e]
Sophie Fourmentin [b].

[a] Laboratoire de Catalyse et Synthèse en Chimie Organique BP 119, Université de Tlemcen, Tlemcen 13000, Algérie.
[b] Unité de Chimie Environnementale et Interaction sur le Vivant (UCEIV, EA 4492), ULCO, 59140 Dunkerque, France.
[c] Centre Universitaire Belhadj Bouchaib, BP 284, 46000 Ain Temouchent, Algérie.
[d] Ecole Supérieure en Génie Electrique et Energétique d'Oran (ESGEE), BP 64 CH2 AchabaHanifi USTO 31000 Oran, Algeria.
[e] Faculté des sciences économiques , BP 226, Université de Tlemcen, Tlemcen 13000, Algérie.

*Email : hanane.chaker@yahoo.fr

Abstract

In the present study, the Box-Behnken design in the response surface methodology (RSM) was availed to investigate the modelization and optimization of Methyl Orange (MO) mineralization parameters. The process was carried out in the presence of lanthanum (La) doped mesoporous titanium dioxide (TiO_2) by a simple impregnation method using various La doping amounts (0.5, 1.5 and 3 wt%). The physico-chemical characteristics of each catalysts are studied under several approaches. The effects of the wavelength of irradiation light, catalysts weight and MO concentration on the yield of MO mineralization were investigated. Based on ANOVA analysis, the results show that the response of MO mineralization (R) in photocatalytic process was significantly affected by a positive individual effect of wavelength and catalyst weight. However, the individual effect of MO concentration

---

[*] Corresponding author

has an antagonist impact through the whole process. The optimum conditions were achieved for the light irradiation wavelength of 310 nm, catalyst weight of 80 mg, and MO concentration of 20 ppm, which allowed reaching 99.89% of mineralization. Overall, the adjusted coefficient of determination (R^2) value of 0.9956 indicated that the used model was quite suitable and the selected RSM was successful in optimizing the mineralization conditions of MO.

1. Introduction

Over the past few years, semiconductor TiO_2 has been widely used in many applications, especially in photocatalytic wastewater treatment processes [1-4]. The photocatalytic activity of TiO_2 can be improved through doping with different types of elements like metals (Au, Ag, Co, etc), non-metals (N, Mg, S, etc.) and rare earths (Ce, La, Eu, etc.)[5-9]. In particular, La, which has the electron configuration of [Xe], i.e. $4f^1 5d^1 6s^2$, is an efficient dopant for improving the photocatalytic properties of TiO_2 because its d and f orbitals are incomplete [10, 11]. It is widely admitted that the presence of La engenders electron trapping and therefore limits their recombination with holes to prevent the formation of electron-hole (e^-/h^+) pairs. This leads to improve the photodegradation efficiency [12, 13]. Furthermore, the presence of La offers several advantages among which is the reduction in the crystallite size, the increase in the number of oxygen vacancies, and the delay in phase transformation of anatase into rutile[12, 14].**Table 1** shows some applications of La-doped TiO_2 in the photodegradation of organic pollutants.

Table 1. Applications of La-doped TiO_2 materials in the photodegradation of organic molecules from the literature

Photocatalysts	Pollutants	Degradation efficiency (%)	Eg (eV)	Reaction conditions	References
TiO_2	Methyl Orange	18	3.2	180 min, visible light, 25ppm, pH=5	[15]
Co-La/TiO_2		98	3.0		

P25		85	3.2	150min, sunlight, 50 ppm, pH=5.	[16]
Anatase		71	/		
0.25%La/	Ibuprofen	67.6	3.35		
TiO_2		81.9	3.15		
0.5%La- TiO_2		93.7	3.01		
1%La- TiO_2		96.9	2.90		
2%La- TiO_2					
TiO_2	Methyl	11	3.2	60 min, visible light, 10 ppm.	[17]
$La^{3+}/Y^{3+}/Eu^{3+}$	Orange	49	/	60 min, visible light,10 ppm.	
co-doped TiO_2		58		60 min, UV irradiation,10 ppm.	
0.5%La/TiO_2	Methyl Orange	98.7	/	120min, UVC irradiated 20 ppm.	[18]
0.1%La/TiO_2	Methyl Orange	82.5 38	2.99	180 min, UVC irradiation, 10 ppm. 180 min, visible light,10 ppm.	[19]
La/N-TiO_2	Methyl Orange	78	3.04	150 min, visible light, 5ppm.	[20]
TiO_2 (P25)	Oily waste Phenol	88 76	/	pH =5.5, full UV light (200–430 nm), [Oily waste] =480±36 , [phenol]=69±15 mg/L	[21]

RSM is one of the most popular experimental design methods applied by researchers in a wide range of fields, especially in chemistry where several parameters are often needed to investigate chemical processes[21-24]. The main purpose of using the RSM is to create an an experiment design that allows achieving the optimal operating conditions. In addition, it is widely acknowledged that RSM is an effective statistical and analytical tool for modeling and optimizing various processes and in various research fields, particularly in photocatalysis[25-27].

It was found that the Box-Behnken experimental design is well suited for the RSM; it is quite appreciated for its fast and economic convergence as compared with the traditional approaches[28, 29]. This technique can provide 3 to 7 factors, along with three levels of experimental conditions (low, medium and high levels) [30, 31]. It is interesting to note that the Box-Behnken design proved to be much more efficient than the other response surface designs. Moreover, it is worth recalling that the experimental design efficiency is actually defined as the number of coefficients in the model under consideration divided by the number of experiments. For example, while the efficiency in the Box-Behnken design is 0.77, it is equal to 0.67 in another center composite design (CCD)[32].

In this study, UV light-driven photocatalysts of lanthanum-doped mesoporous TiO_2 were successfully prepared by a common impregnation method using various La doping amounts (0.5, 1.5 and 3wt %). The photocatalytic activity of the prepared photocatalysts was evaluated in the mineralization of MO under UV light irradiation. Then, the impacts of three parameters, namely the light irradiation wavelength, catalyst weight and pollutant concentration, on the photocatalytic process are investigated by the Box-Behnken design. Further, analysis tried also to determine the interactions between the parameters under consideration, as well as the optimal operating conditions for the process to be carried out. This leads to considerably reduce the number of required tests. It should be pointed out that the main advantage of this approach lies in its capacity to help save time and money in industrial processes.

2. Experimental work

2.1. Reagents

Titanium isopropoxide (IV)[$C_{12}H_{28}O_4Ti$, (97%)], acetic acid [CH_3COOH, (20%)], Pluronic P123 [$EO_{20}PO_{70}EO_{20}$, 99.99%], Lanthanum nitrate hexahydrate [$La(NO_3)_3.6H_2O$, (99,99%)], Ethanol [C_2H_5OH, (99%)], Methyl orange [$C_{14}H_{14}N_3NaO_3S$, >98%]. Every chemical product were purchased from Sigma Aldrich.

2.2. Synthesis of materials

Mesoporous TiO_2 was prepared by the hydrothermal-assistant sol-gel method [33]. To do this, 5g of titanium isopropoxidewere added dropwise to the acetic acid solution (20%). The suspension (Solution 1) obtained was stirred for 4h. Next, Solution 2, which was prepared by adding 3g of Pluronic P123 triblock copolymer into 20 mL of ethanol, was added drop by drop to Solution 1. The resulting suspension was stirred for 24h at room temperature. The solution obtained was transferred into a Teflon autoclave which was placed in an oven at 100°C for 48h. Afterwards, it was taken out of the oven to cool down to room temperature. As a next step, the solution was filtered, and the resulting solid was washed with distilled water several times. Evaporation of the remaining water took place at the temperature of 80°C, during 24h. Finally, the recovered solid was calcined at 500°C for 4h, at the heating rate of 1°C/min and a cooling rate of 1°C/min, to obtain the mesoporous TiO_2 material. On the other hand, La with different amounts, i.e. 0.5, 1.5 and 3%, was impregnated on calcined mesoporous TiO_2 by means of the incipient wetness impregnation technique using lanthanum nitrate [8]. Briefly, the calcined mesoporous TiO_2 was mixed with an aqueous solution of lanthanum nitrate in a rotatory evaporator, at 60°C, and for a period of 2h. The resulting suspension was first dried at 80°C for 24h and then calcined in air at 400°C for 4h at a heating rate of 1°C/min and a cooling rate of 1°C/min, to obtain 0.5, 1.5 and 3% La/TiO_2.

2.3. Characterization method

The X-ray powder diffraction (XRD) patterns were recorded on a RigakuD/max2500 diffractometer, using CuKαradiation (λ =1.541874 A), with an acquisition time of 1 s, in the range of 2θ = 20°- 80°, in steps of 0.02°/min. In addition, the surface area and pore size analysis of the samples were carried out through nitrogen adsorption–desorption measurements on a Quantachrome NOVA1000 Series instrument, at the temperature of -196°C.The prepared catalysts overnight at 250°C, under vacuum. In addition, the UV-Vis reflectance diffuse (RD/UV-Vis) spectra of the catalysts were recorded on a Varian Cary 100 Scan UV–Vis Spectrophotometer equipped with an integrating sphere accessory in the diffuse reflectance mode (R). Note that the inorganic compound of Barium sulfate ($BaSO_4$) was used as the reference material.

2.4. Photocatalytic properties

The photocatalytic properties of the prepared catalysts were evaluated through the photodegradation of MO ([MO]=30ppm,$m_{catalyst}$=20 mg, $V_{solution}$=100 mL for preliminary tests). The tests were carried out in a MULTIRAYS photoreactor (Heliosquartz, Italy) (**Figure 1**) that was fitted with ten exchangeable UV lamps (15 W each): (UVC, 254 nm), (UVB, 310 nm) and (UVA, 366 nm). For the most optimal catalyst, a series of experimental parameters, involved in the photodegdation and mineralization of MO, were chosen for the described modeling approach. For this, the studied solution was kept in darkness under stirring for 30 min, until the adsorption/desorption equilibrium was reached. Then, this solution was irradiated, and samples were taken every 5min. For each sample, the measurement of absorbance was made at λ= 463 nm, using the Perkin Elmer Lambda 2S spectrophotometer. Note that each test was repeated three times. At the end of the experiment, the total organic carbon (TOC) content was measured by means of a Shimadzu TOC–VCSH analyzer. The same procedure was repeated for all the catalysts previously prepared.For the recyclability experiments, the optimal material was reused (6 times) after drying at 80°C.

Fig. 1. Schematic of photocatalysis experiment.

The following equation was used to calculate the yield (%) for the TOC conversion:

$$\text{Yield}(\%) = \frac{C_0 - C_{residue}}{C_0} * 100 \qquad \boldsymbol{Eq.1}$$

Where C_0 is the initial TOC concentration and $C_{residue}$ is the TOC concentration at the end of the experiment.

2.5. Box-Behnken design

Broadly speaking, the photocatalytic process depends on several operating parameters. For better monitoring the experiments, the photocatalytic reactions were designed on the basis of an experimental approach through the use of the most optimal catalyst. Furthermore, the empirical quadratic polynomial model was used, and all the experimental data were compiled by means of the Box-Behnken design using the Design-Expert Software, Version 12.0.3.0, from Stat-Ease, Inc. It is worth mentioning that the Box-Behnken design is a factorial combination of a minimum of three parameters with incomplete block designs. In each block, one factor is held at the central point, while the others vary according to four different combination values with respect to the upper and lower limits[34]. The experiments were conducted according to a three level scale, i.e. low (-1), central (0) and high (+1). Note that one level was set for each variable (**Table 2**). It is worth recalling that the independent variables in this experiment were the light irradiation wavelength λ (nm), catalyst weight m (mg) and MO concentration [MO] (ppm), labeled X_1, X_2 and X_3, respectively. Therefore, the total number of experiments to be carried out was 15. It may be calculated as follows[35]:

$$N = k^2 + k + cp \qquad \boldsymbol{Eq.2}$$

Where k is the factor number and cp is the replicate number of the central point[36, 37].

The coded values of the independent variables were obtained using the Equation 3[28]:

$$x_i = \frac{X_i - X_{io}}{\Delta X_i} \qquad i = 1,2,3,\ldots..k \qquad \boldsymbol{Eq.3}$$

Where x_i are the coded values, X_i the real values of independent variables, X_{io} is the real value in the center plane, and ΔX_i the step change. Moreover, a polynomial regression model was utilized to analyze the causal relationship between the dependent and independent variables. The regression equation was expressed as follows:

$$Y = \beta_0 + \sum_{i=1}^{K} \beta_i x_i + \sum_{i=1}^{K} \beta_{ii} x_i^2 + \sum_{i=1}^{K-1} \sum_{j=2}^{K} \beta_{ij} x_i x_j + \mathcal{E} \qquad \boldsymbol{Eq.4}$$

Where Y is a response variable, β represents a set of regression coefficients (also called constants), k is the number of exogenous variables (independent variables), and Ɛ an unknown constant error vector.

It must be noted that the positive sign in the regression equation represents the synergistic effect between parameters, whereas the negative sign indicates an antagonistic effect. The optimal values of the parameters were obtained through the estimation of the regression equation and the interpretation of the response of the contour plots.

Table 2. Experimental ranges and levels of independent variables

Variables design	Factors	Range and levels		
		-1	0	1
X_1	λ (nm)	254	310	366
X_2	$m_{catalyst}$ (mg)	20	50	80
X_3	[MO] (ppm)	20	40	60

3. Results and discussions

3.1. Physicochemical properties of the prepared materials

3.1.1. X-ray diffraction characterization

Figure 2 shows the XRD spectra of TiO_2 and X%La/TiO_2 materials. For all the samples, it seems that TiO_2 is present in the anatase phase (JCPDS Files No.21-1272) with a crystallite size around 12 nm, as calculated using the formula of Debye Scherrer given by Equation 5:

$$d = \frac{0.98 * \lambda}{\beta * cos(\Theta)} \qquad \boldsymbol{Eq.5}$$

Where d is the crystallite size (nm), λ the wavelength of light (nm), β the full width at half maximum (FWHM) (Rad), and θis Bragg's angle (Rad) corresponding to the most intense peak characteristic of TiO_2; this peak is located at 25°.

On the other hand, no characteristic peak of La species was found in the recorded XRD patterns, implying that either La ions were incorporated into the bulk of mesoporous TiO_2, or the La particles were very small and highly dispersed on the mesoporous TiO_2 surface. Note that the ionic radius of La^{3+} (1.15A°) is bigger than that of Ti^{4+} (0.68A°) [5, 10], which indicates that these lanthanide ions cannot really be incorporated within the lattice structure of TiO_2 [5, 10].

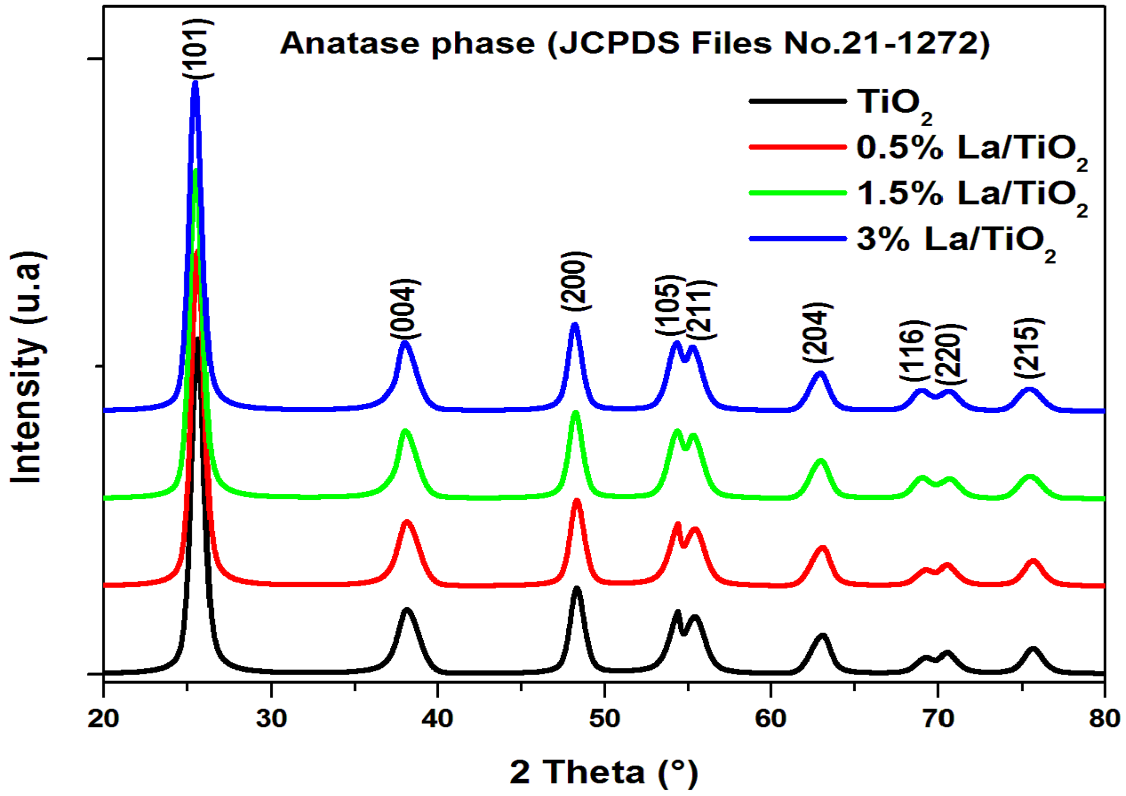

Fig. 2. XRD patterns of TiO_2 and X% La/TiO_2 materials.

3.1.2. RD/UV-Vis characterization

Figure 3 displays the RD/UV–Vis spectra of the prepared materials. All samples show an important absorption within the UV range (< 400 nm) [38-40]. Besides, **Figure 4** indicates that the deconvolution spectra of mesoporous TiO_2 shows the presence of intense absorbance bands around 210-250 nm and 300-350 nm. The first region might be associated with the ligand–metal charge transfer between tetrahedral Ti^{4+} and an oxygenated ligand such as O^{2-}, while the second one is ascribed to the Ti^{4+}cations in the octahedral environment and to the anatase phase as well[38-40].

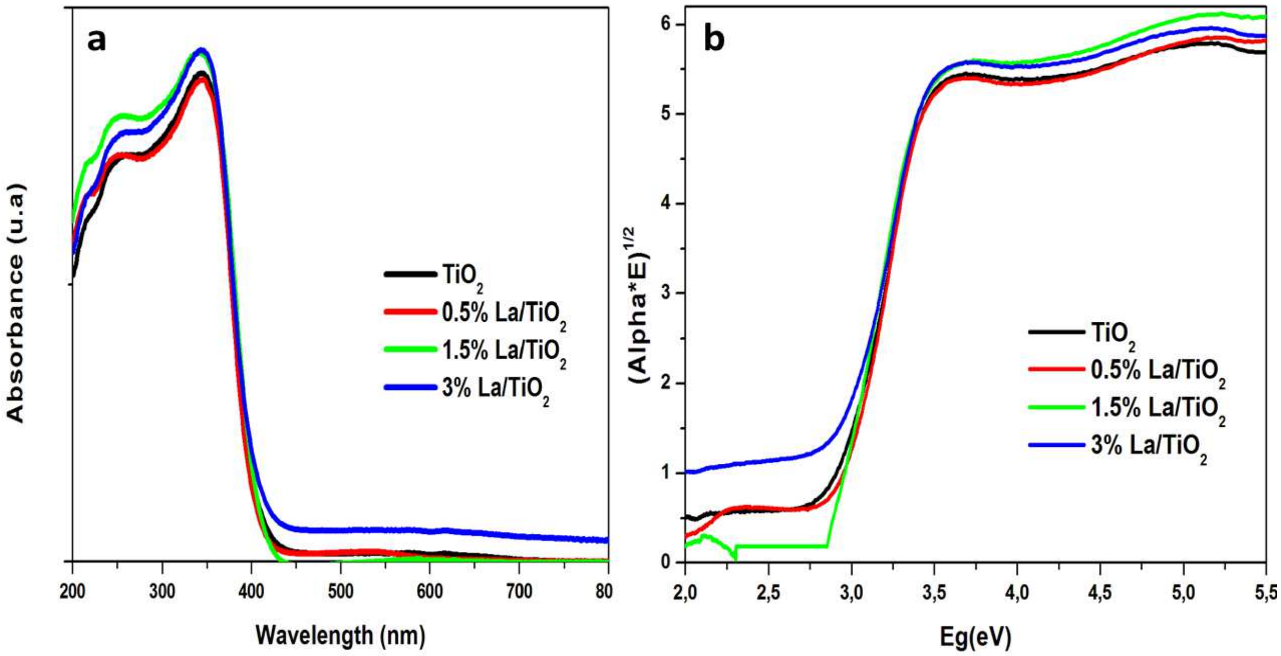

Fig. 3. (**a**) RD/UV-Vis absorption spectra and (**b**) the variation of $(\alpha{*}E)^{1/2}$ as a function of E_g of TiO_2 and X %La/TiO_2 materials.

It can clearly be seen that the intrinsic absorption band of La-doped TiO_2, unlike the undoped TiO_2, shifts towards the infrared region. The absorption band changes with the doping levels, and the red shift is greater when the quantity of La is important. The improvement in the La-doped mesoporous TiO_2 absorption in the visible region of the UV-Vis spectra may be assigned to the creation of a new energy level near the conduction band of TiO_2 (**Figure 8**)[8, 9]. This energy level makes the transition of electrons from the valence band to the conduction band of TiO_2 much easier and consequently promotes the absorption of long-wave photons, which causesthe red shift to move into the UV-Visible spectra[11, 41-43].

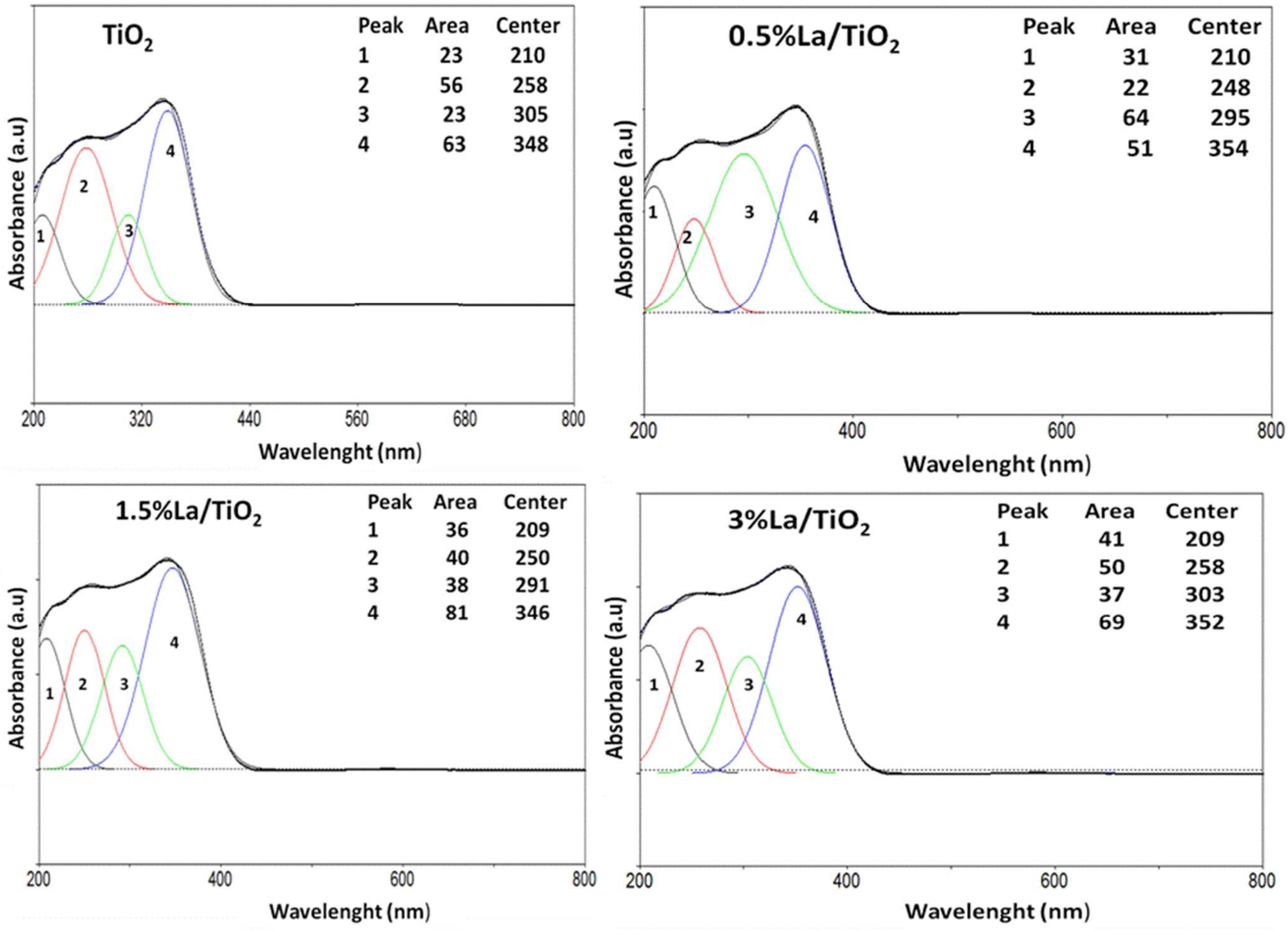

Fig .4. Deconvolution of RD/UV-Vis spectra of TiO_2 and X %La/TiO_2 materials.

Figure 3 depicts the reflectance diffuse spectra that were recalculated from the graph representing the variation of $(\alpha E)^{1/2}$ as a function of the energy in order to obtain the band gap energy values (E_g). These values were determined by extrapolation of the straight line representing $(\alpha E)^{1/2}$as a function of E_g to zero. **Figure 3.b** clearly suggests that the presence of La^{3+}induces a decrease in the band gap energy value of pure TiO_2 as the amount of Lanthanum (**Table 3**) this proves the success doping of La in TiO_2 support.

Table 3. Structural and optical characteristics of the materials prepared

Materials	S_{BET}($m^2.g^{-1}$)	Pore volume (cc/g)	Pore diameter (nm)	Eg(eV)
TiO_2	102	0.20	2.8	2.88
0.5%La/TiO_2	123	0.27	2.9	2.86
1.5%La/TiO_2	130	0.30	3.1	2.82
3%La/TiO_2	215	0.33	3.5	2.78

3.1.3. Textural properties

Nitrogen adsorption and desorption analyses were carried out for all materials, and the results obtained are illustrated in **Figure 5**. The shape of all isotherms indicates that these are of type IV; these isotherms are characteristic of mesoporous materials[8, 9]. However, a typical hysteresis B behavior is clearly observed in all materials. Furthermore, the shapes of the isotherms and hysteresis suggest the presence of slit-like pores which are thus considered to account for the large surface areas of photocatalysts. It is important to mention that the measured surface area using BET (Brunauer-Emmett-Teller) method **(S_{BET})** of the materials was found equal to 102 $m^2.g^{-1}$ for undoped TiO_2,123 $m^2.g^{-1}$ for 0.5%La/TiO_2, 130 $m^2.g^{-1}$ for 1.5% La/TiO_2, and 215 $m^2.g^{-1}$for 3% La/TiO_2, as shown in **Table 3**. These results suggest that there is a clear tendency for the surface area of materials to increases with the amount of the dopant La goes up. It is worth noting that the La particles contribute to the increase of the specific surface due to the good distribution of these particles and to their small size as well [9].

Furthermore, the pore size distribution curves of the samples were determined according to the BJH (Barrett, Joyner, Halenda) method, are shown in **Figure 5**. In all cases, the intense peak that is centered at around 2-4 nm indicates that the pores have an average size of 3 nm. The increase in the specific surface of the doped materials may be attributed to the introduction of La particles in the TiO_2 pores and consequently increase the pore size.

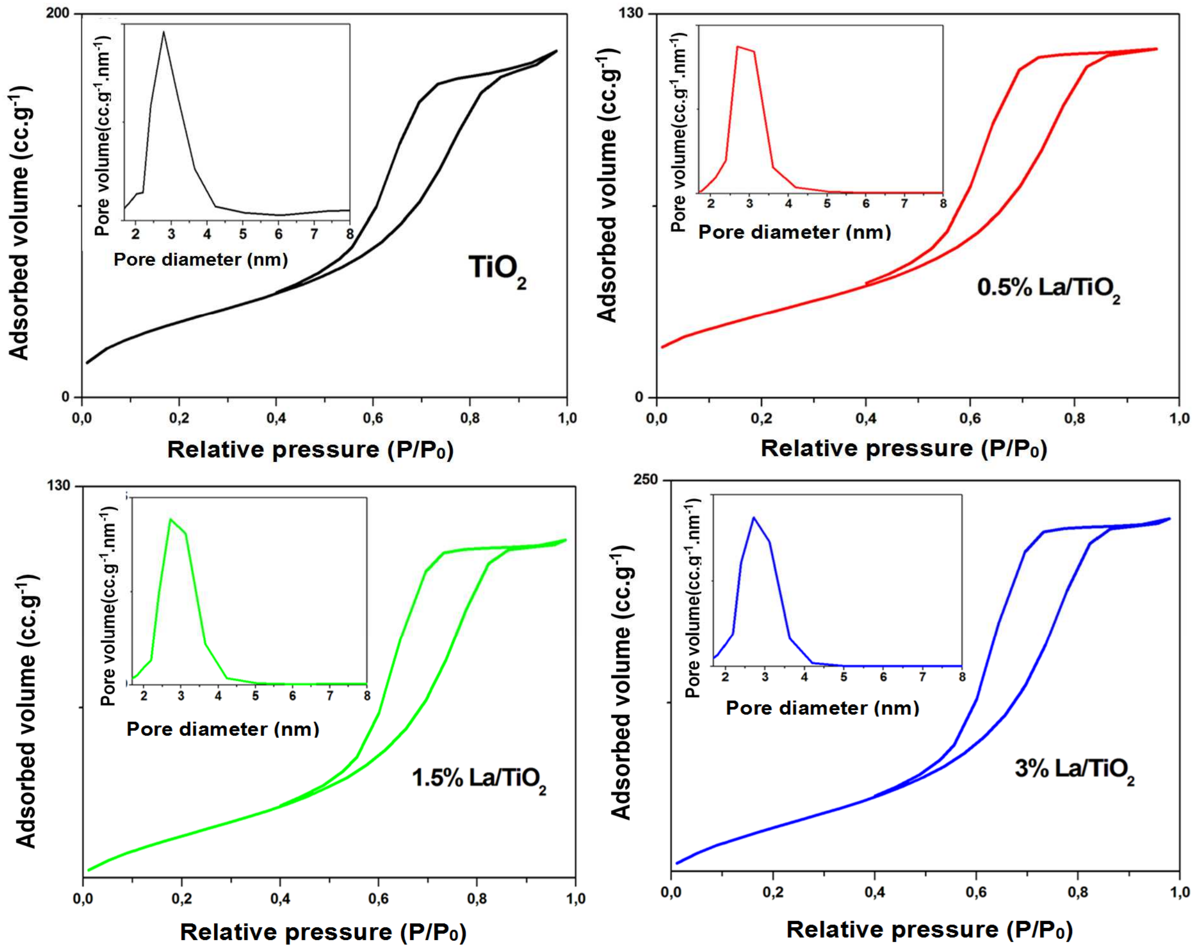

Fig. 5. Nitrogen adsorption-desorption isotherms and pore size distribution of X%La/TiO$_2$ at 77K.

3.2. Photocatalytic test

First, preliminary tests were carried out for the purpose of selecting the optimal content of lanthanum, and then a comprehensive study was conducted on the optimal catalyst. To do this, the photocatalytic activities of the prepared photocatalysts were evaluated via the photodegradation and mineralization of MO in aqueous solution under UV-Vis light irradiation, as illustrated in **Figures 6.a, 6.b and 6.c**. The photodegradation of MO was followed by light absorption, at regular time intervals, as indicated in the experimental section. In the absence of irradiation and catalysts, only a slight light absorption was observed (less than 2%). The results obtained indicate that both light and the catalyst are necessary for an efficient MO photodegradation. Interestingly, the strong absorption band of MO, located at λ = 463 nm, decreased as the number of irradiation times went up; this band finally almost disappeared within 25min when 3%La/TiO_2 was used as a photocatalyst.

Furthermore, **Figures 6.a, 6.b and 6.c** suggest that the photodegradation of MO by La-doped mesoporous TiO_2 is more efficient than by pure TiO_2, whatever the light source. The photocatalytic activity of the prepared photocatalysts, under UV light irradiation, follows the decreasing order of 3%La/TiO_2 >1.5%La/TiO_2 >0.5%La/TiO_2 >TiO_2. Furthermore, it turned out that the photodegradation of MO by La-doped mesoporous TiO_2 was faster under UVA irradiation and varied with the type of light source (UVA> UVB>UVC); this was not the case for pure TiO_2 for which the photodegradation activity followed the increasing order UVA < UVB < UVC. It has been largely proven that TiO_2 is more active under UVC irradiation; this is mainly attributed to its wide band gap[8, 9].

The stability of the most performant catalyst, i.e. 3%La/TiO_2, was assessed during six cycles. It is useful to know that, after each cycle, the catalyst was recovered by centrifugation, dried and reused. In addition, it is worth mentioning that MO photodegradation remained almost unchanged, between 95 and 98% (**Figure 6.d**).

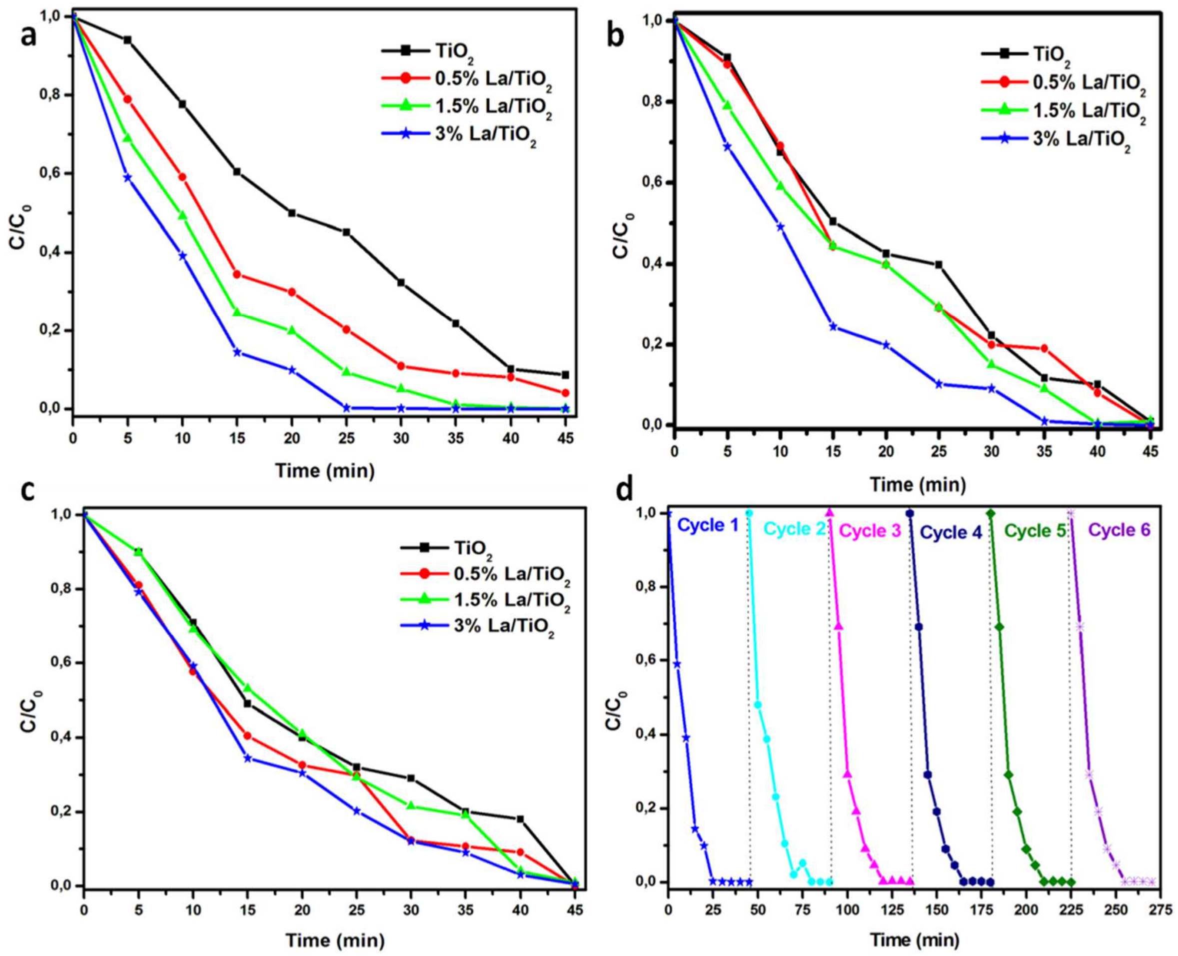

Fig. 6. (**a**), (**b**) and (**c**) Photodegradation curves of MO using pure and doped mesoporous TiO_2 photocatalysts under UVC, UVB and UVA irradiations respectively. (**d**) Stability test result of 3%La/TiO_2 photocatalyst after 6 cycles.

To investigate the total mineralization efficiency of prepared photocatalysts, TOC measurements were undergone. In fact, the disappearance of the MO coloration is not enough to prove its mineralization. The degradation of the organic dye leads to organics by-products that will be degraded their turn. These compounds are no more colored and only TOC measurements can prove their effective degradation[9].

The mineralization yields calculated after 30 min of irradiation are illustrated in Figure 7. The TOC abatement values were significantly higher for La-doped mesoporous TiO_2 whatever the light source. The best TOC abatement was 99.80% for 3%La/TiO_2. These results indicate that La loading enhanced the photocatalytic activity of TiO_2 and its mineralization efficiency.

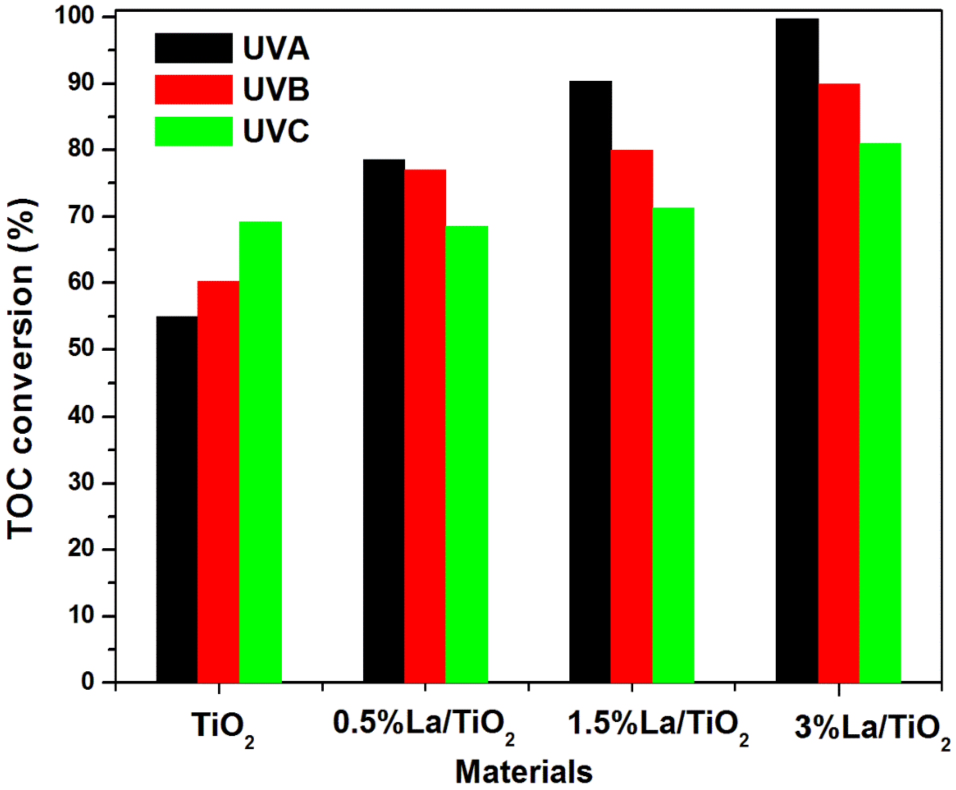

Fig. 7. TOC conversion (%) for the photocatalytic degradation of MO under UV light irradiation.

It should be noted that the highest photocatalytic activity was obtained with 3%La-doped TiO_2, for all light wavelengths. This could be explained by the transition of the electrons of the 4f subshell of lanthanum ion, which leads to the improvement of the optical properties of the photocatalyst. They support the separation of photo-generated electron-hole (e^-/h^+) pairs. Furthermore, the red shift of the optical adsorption edge of TiO_2 by lanthanum-doped TiO_2 was useful for the improvement of the UV-light photocatalytic activity of TiO_2. In this context, Stengl et al. found out that the optimum content of lanthanum supported on oxides for the photodegradation of azo dyes was ~3–4 wt% under UVC irradiation, while the optimum content of lanthanum was around 1–2 wt% under visible light irradiation [44]; these results are in good agreement with our findings. It is useful to recall that increasing the dopant ion content induces a higher surface barrier and a narrower space charge region.

3.3. Proposed photocatalytic mechanism

TiO_2 is a semiconductor with a large band gap. Nevertheless, the biggest problem of using TiO_2 lies in the fact that only UV light irradiation can be applied because, as stated before, this material possesses a wide band gap. This drawback was addressed through the doping of TiO_2 with La, which allowed reducing the band gap width.

Hence, La-doped TiO_2 was capable of absorbing photons from visible light, and the electrons were excited from the valence band (VB) to the conduction band (CB) of the semiconductor (Figure 8), hence creating electron-hole pairs (e^- and h^+), as shown in reaction 1. It is worth noting that the holes created in the VB can therefore form hydroxyl radicals ($OH^•$) via the oxidative reactions, expressed in reaction 2.

(i) Light (appropriate spectrum) + La-doped TiO_2 $\longrightarrow$ La-doped TiO_2 (h^++e^-)   Reaction 1

(ii) Oxidative reactions with holes

$$h^+ + H_2O \longrightarrow H^+ + OH^• \quad \textbf{Reaction 2}$$

$$2h^+ + 2H_2O \longrightarrow 2H^+ + H_2O_2 \quad \textbf{Reaction 3}$$

$$H_2O_2 \longrightarrow OH^• + OH^• \quad \textbf{Reaction 4}$$

(ii) Reductive reaction with O_2

$$2e^- + O_2 \longrightarrow O_2^{•-} \quad \textbf{Reaction 5}$$

$$O_2^{•-} + 2H^+ \longrightarrow H_2O_2 + O_2 \quad \textbf{Reaction 6}$$

$$H_2O_2 \longrightarrow OH^• + OH^• \quad \textbf{Reaction 7}$$

$$MO + OH^• \longrightarrow \text{Mineralized products} \quad \textbf{Reaction 8}$$

Consequently, the electrons in the CB form super oxide radical anions ($O_2^{•-}$) through the reductive reactions, as given in reactions 5 and 6. It is important to note that the two radicals $OH^•$ and $O_2^{•-}$ are strong oxidants that can oxidize the organic compounds. Indeed, $O_2^{•-}$ has a sufficient reduction potential that allows oxidizing organic species with strong electron-donating groups (such as active azo -N=N- bond); however, radical $OH^{\bullet}$ tends to remove hydrogen or attack the C-C unsaturated bonds [45]. Therefore, a model pollutant containing unsaturated C-C bonds such as MO can very likely be photocatalytically oxidized or attacked with the formation of $OH^{\bullet}$ radicals.

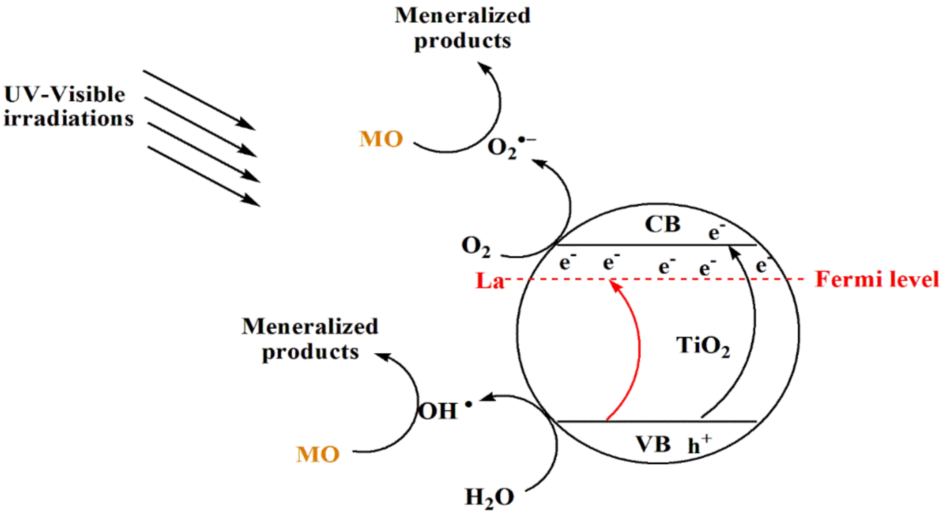

Fig. 8. Proposed pathway for photocatalytic degradation of MO using La-doped TiO_2 under UV irradiation[46].

3.4. Experimental design and statistical analysis

The Box–Behnken design matrix for the real values, along with the experimental (irradiation at 30 min) and predicted values for TOC abatement (%) for the optimum photocatalyst are summarized in **Table 4.** The maximum abatements (%) were found equal to 99.89% and 100% for actual and predicted values, respectively.

The final quadratic equation (**Equation 6**) generated by the design model with the three independent variables and dependent responses (Y) can be expressed as:

$$\widehat{Y2} = 71.7667 + 2.8625(X_1) + 22.4437(X_2) - 11.6663(X_3) + 0.3(X_1)(X_2) - 0.475(X_1)(X_3) + 1.0875(X_2)(X_3) + 5.60792(X_1)^2 - 6.17458(X_2)^2 + 2.60042(X_3)^2 \quad \textbf{Eq. 6}$$

Table 4 . Box-Behnken design with experimental values for the independent variables

	Codedlevel of Variables			Actuallevel of variables			R (%)	
Run order	**X_1**	**X_2**	**X_3**	**X_1**	**X_2**	**X_3**	**Observed response**	**Predicted response**
1	0	1	-1	310	80	20	99.89	100
2	-1	0	1	254	50	60	65.9	65.92
3	0	-1	-1	310	20	20	59	58.50
4	-1	1	0	254	80	40	91	90.48
5	0	1	1	310	80	60	79.56	80.05
6	1	0	-1	366	50	20	95	94.97
7	1	-1	0	366	20	40	50.8	51.31
8	0	0	0	310	50	40	71	71.80
9	0	0	0	310	50	40	72	71.76
10	-1	0	-1	254	50	20	89	88.30
11	0	0	0	310	50	40	72.3	71.76
12	0	-1	1	310	20	60	34.21	32.99
13	-1	-1	0	254	20	40	45	46.19
14	1	0	1	366	50	60	70	70.69
15	1	1	0	366	80	40	98	96.80

The model statistical significance and its validity were tested through the analysis of variance (ANOVA). The model robustness was evaluated using both the coefficient of determination (R^2) and the adjusted coefficient of determination (adjusted R^2). They were both found equal to 0.9956 approximatively (**Figure 9**).

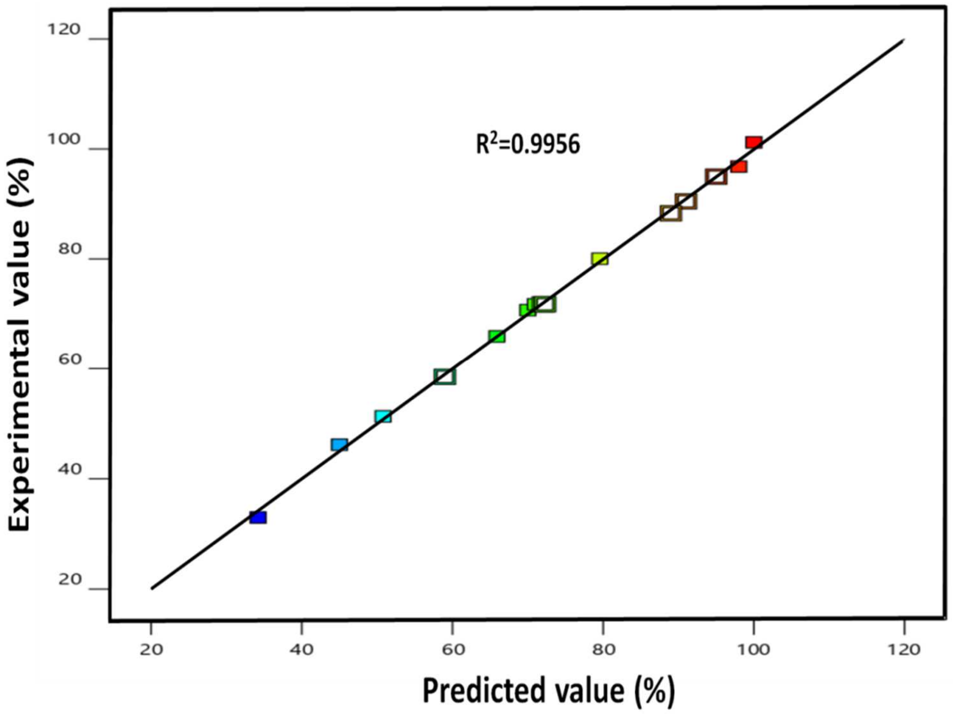

Fig. 9. Predicted response vs. observed response

Conventionally, the commonly accepted threshold value is equal or greater than 0.80. The closer this value is to one, the more suitable the model is[47]. As it can be seen in **Table 5**, the Fischer value (*F*-value) and probability value *(p*-value) of the yields were quite significant as they were found smaller than 0.05%.

Table 5. Analysis of Variance for Response surface quadratic model

Source	**Sum of Squares**	**Df**	**Mean Square**	**F-value**	**p-value**	
Model	9	9	610.49	349.53	< 0.0001	**Significant**
X_1	65.55	1	65.55	37.53	0.0017	
X_2	4029.78	1	4029.78	2307.25	< 0.0001	
X_3	1088.81	1	1088.81	623.40	< 0.0001	
X_1X_2	0.3600	1	0.3600	0.2061	0.6689	
X_1X_3	0.9025	1	0.9025	0.5167	0.5044	
X_2X_3	4.73	1	4.73	2.71	0.1607	
X_1^2	116.12	1	116.12	66.48	0.0005	
X_2^2	140.77	1	140.77	80.60	0.0003	
X_3^2	24.97	1	24.97	14.30	0.0129	
Residual	8.73	5	1.75			
Lack of Fit	7.81	3	2.60	5.62	0.1549	**not significant**

R^2=0.9984, Adj. R^2 =0.9956 and Pred. R^2= 0.9769.

Furthermore, the sum of squares (SS) taken from ANOVA data were used to calculate the total percentage contributions (TPC) for each model term. The TPC for the first order, interaction, and quadratic terms could be obtained using the following three equations[48]:

$$TPC_i = \frac{\sum_{i=1}^{n} SS_i}{\sum_{i=1}^{n}\sum_{i=1}^{n} SS_i + SS_{ii} + SS_{ij}} \times 100 \qquad \boldsymbol{Eq.7}$$

$$TPC_{ij} = \frac{\sum_{i=1}^{n}\sum_{i=1}^{n} SS_{ij}}{\sum_{i=1}^{n}\sum_{i=1}^{n} SS_i + SS_{ii} + SS_{ij}} \times 100 \qquad \boldsymbol{Eq.8}$$

$$TPC_{ii} = \frac{\sum_{i=1}^{n}\sum_{i=1}^{n} SS_{ii}}{\sum_{i=1}^{n}\sum_{i=1}^{n} SS_i + SS_{ii} + SS_{ij}} \times 100 \qquad \boldsymbol{Eq.9}$$

This can be expressed as the factorial weight or the variance part taken by each considered factor. As shown in **Figure 10**, the individual effect is more predominant than the interactive and quadratic effects, which is consistent with the findings reported in the literature[29]. Furthermore, the catalyst weight can be considered as the most important factor, followed by the MO concentration. However, the light irradiation wavelength is less decisive in our model.

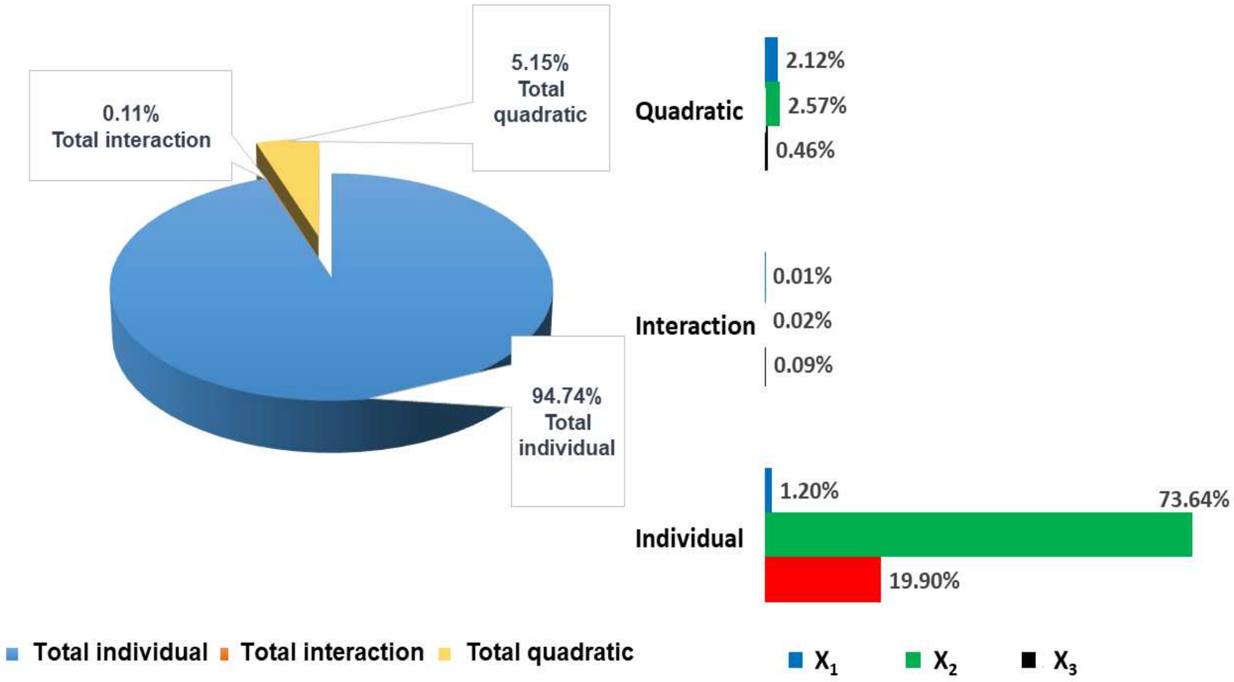

Fig. 10 .Schematic representation of the Percentage Contribution.

Based on the data obtained by ANOVA for the quadratic model (**Table 5**), the F-value of the Lack of Fit (LOF) equal to 5.62 implies that the LOF is quite low as compared to the absolute error. A non-significant LOF value means that the contribution of the selected variable is sufficiently high for building the entire model. Therefore, it can be stated that our results are in good agreement with those reported in several works in the relevant literature [48, 49].

Finally, three dimensional response surface plots are drawn in **Figure 11** to visualize the interaction effects between the independent variables and the responses.

3.5. Optimization and model validation

Figure 11 presents the three dimensional (3D) response surface plots of yields as a function of the independent variables. The 3D surface explains the relationship between the dependent variables (R) and independent variables (X_1, X_2 and X_3). With regard to these three variables, one of them remained constant at its zero level, while the two others were analyzed separately.

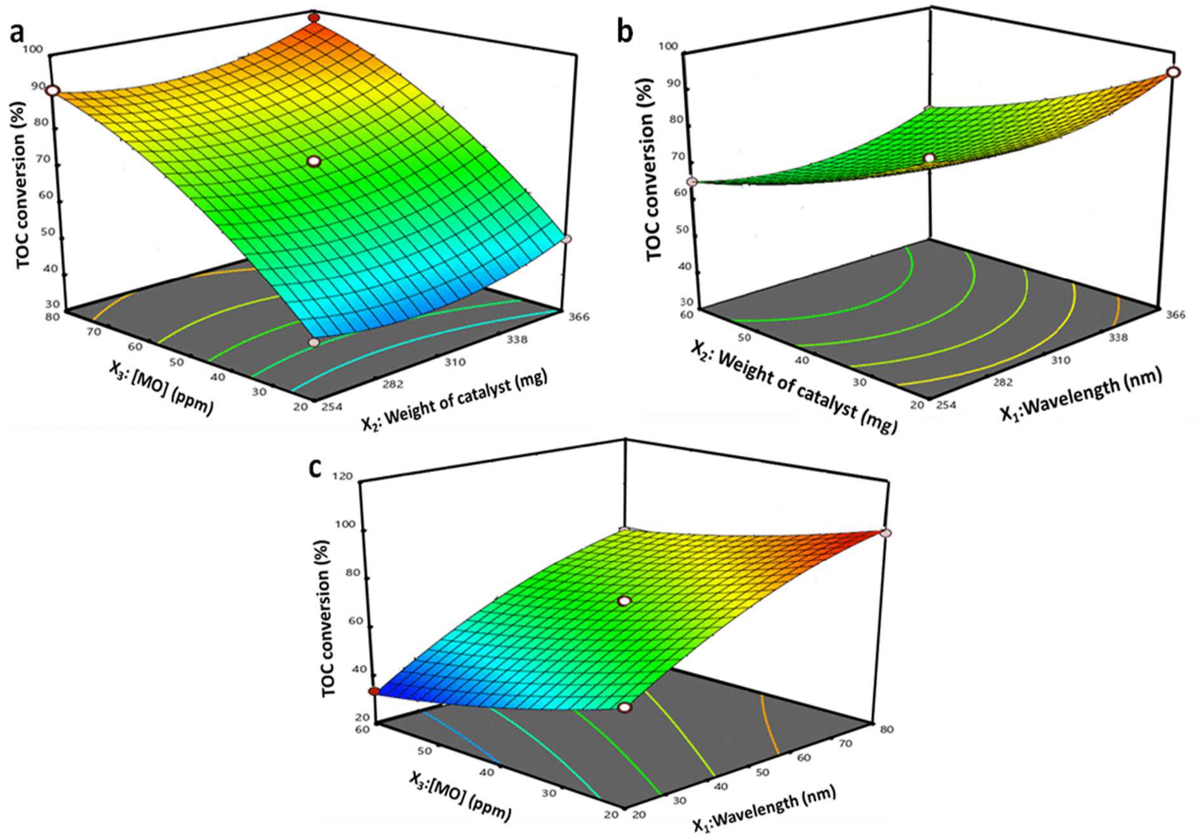

Fig. 11. 3D surface plots of R as a function of **(a)** X_2 and X_3, **(b)** X_1 and X_2, and **(c)** $X_2$and X_2

Figure 11.a shows the contour plot of response R as a function of the MO concentration and catalyst weight, while the irradiation light wavelength is kept constant. It is worth indicating that increasing the MO concentration and catalyst weight leads to increase TOC conversion. Similarly, **Figure 11.b** suggests that when the irradiation wavelength and catalyst weight increase, the R value goes up too. Unlike the other observations made in **Figure 11.b**, increasing the irradiation light wavelength and MO concentration, while the catalyst weight is kept constant, results in a decrease of the response R (**Figure 11.c**).

However, it should be noted that there is an upper threshold for the yield optimization levels for these parameters. This finding goes in the same way with the experimental results obtained for other response surfaces works [46-48].

4. Conclusion

This work was mainly focused on the preparation and characterization of nanomaterials based on mesoporous TiO_2 doped with Lanthanum. Besides, it include a modeling and optimization framework for the photodegradation and mineralization of MO under UV light irradiation. The effects of the three parameters, namely the irradiation light wavelength, catalyst weight and pollutant concentration on the mineralization of MO, were studied using the Box-Behnken experimental design. The results of the photocatalytic experiments showed that the 3%La/TiO_2 photocatalyst enhances the photocatalytic activity of TiO_2 under UV irradiation. The activity improvement of TiO_2 can be attributed to the large specific area, good dispersion of La particles, small size of crystallites, and narrow energy gap, which can likely lead to the total elimination of MO. The ANOVA data for the quadratic model revealed that the catalyst weight is the most significant factor influencing the response followed by the pollutant concentration, and finally the irradiation wavelength. Therefore, the quadratic models using the Box-Behnken design are quite as they express a very high coefficient of determination R^2 (0.9956). The optimal conditions after the regression analysis were achieved with an irradiation wavelength of 310 nm, catalyst weight of 80 mg and MO concentration of 20 ppm, for a TOC abatement rate of 98.89%. This study confirms that the Box-Behnken design could be efficiently applied for modeling the MO mineralization process under UV light irradiation using 3%La/TiO_2. Furthermore, this strategy is an interesting economic approach to obtain the targeted information in a short time, with a minimum number of experiments.

CRediT authorship contribution statement

Hanane Chaker Writing - Review & Editing, Conceptualization, Validation, Investigation, Methodology. **Nawal Ameur** Resources, Investigation, Formal analysis, Validation. **Karima Saidi-Bendahou :** Project administration. **Mustapha Djennas:** Methodology, Formal analysis. **Sophie Fourmentin :** Project administration, Supervision.

Declaration of Competing Interest

The authors declare that they have no conflict of interest.

Acknowledgements

The authors are grateful to PHC Maghreb n°27959PD for financial support and would like to thank the Algerian DGRST-MESRS, and the University of Tlemcen and Littoral-Côte-d' Opale for funding this work.

References

[1] Y. Zhang, P. Li, Porous Zr-doped SiO_2 shell/TiO_2 core nanoparticles with expanded channels for photocatalysis, Materials & Design, 88 (2015) 1250-1259.https://doi.org/10.1016/j.matdes.2015.09.093

[2] R. Verma, S. Singh, M. Dalai, M. Saravanan, V.V. Agrawal, A.K. Srivastava, Photocatalytic degradation of polypropylene film using TiO_2-based nanomaterials under solar irradiation, Materials & Design, 133 (2017) 10-18.https://doi.org/10.1016/j.matdes.2017.07.042

[3] Y. Zhang, H. Ma, M. Yi, Z. Shen, X. Yu, X. Zhang, Magnetron-sputtering fabrication of noble metal nanodots coated TiO_2 nanoparticles with enhanced photocatalytic performance, Materials & Design, 125 (2017) 94-99.https://doi.org/10.1016/j.matdes.2017.03.084

[4] A.K. Tareen, K. Khan, M. Aslam, X. Liu, H. Zhang, Confinement in two-dimensional materials: Major advances and challenges in the emerging renewable energy conversion and other applications, Progress in Solid State Chemistry, (2020) 100294.https://doi.org/10.1016/j.progsolidstchem.2020.100294

[5] A.-W. Xu, Y. Gao, H.-Q. Liu, The Preparation, Characterization, and their Photocatalytic Activities of Rare-Earth-Doped TiO_2 Nanoparticles, Journal of Catalysis, 207 (2002) 151-157.doi:https://doi.org/10.1006/jcat.2002.3539.

[6] Y. Xie, C. Yuan, Visible-light responsive cerium ion modified titania sol and nanocrystallites for X-3B dye photodegradation, Applied Catalysis B: Environmental, 46 (2003) 251-259.doi:https://doi.org/10.1016/S0926-3373(03)00211-X.

[7] K.V. Baiju, C.P. Sibu, K. Rajesh, P.K. Pillai, P. Mukundan, K.G.K. Warrier, W. Wunderlich, An aqueous sol–gel route to synthesize nanosized lanthana-doped titania having an increased anatase phase stability for photocatalytic application, Materials Chemistry and Physics, 90 (2005) 123-127.doi:https://doi.org/10.1016/j.matchemphys.2004.10.024.

[8] S. Khaoulani, H. Chaker, C. Cadet, E. Bychkov, L. Cherif, A. Bengueddach, S. Fourmentin, Wastewater treatment by cyclodextrin polymers and noble metal/mesoporous TiO_2 photocatalysts, Comptes Rendus Chimie, 18 (2015) 23-31.https://doi.org/10.1016/j.crci.2014.07.004.

[9] H. Chaker, L. Chérif-Aouali, S. Khaoulani, A. Bengueddach, S. Fourmentin, Photocatalytic degradation of methyl orange and real wastewater by silver doped mesoporous TiO_2 catalysts, Journal of Photochemistry and Photobiology A: Chemistry, 318 (2016) 142-149.https://doi.org/10.1016/j.jphotochem.2015.11.025.

[10] F.B. Li, X.Z. Li, C.H. Ao, S.C. Lee, M.F. Hou, Enhanced photocatalytic degradation of VOCs using Ln^{3+}–TiO_2 catalysts for indoor air purification, Chemosphere, 59 (2005) 787-800.
doi:https://doi.org/10.1016/j.chemosphere.2004.11.019.

[11] Z. Shi, X. Zhang, S. Yao, Synthesis and photocatalytic properties of lanthanum doped anatase TiO_2 coated Fe_3O_4 composites, Rare Metals, 30 (2011) 252-257.doi:https://doi.org/10.1016/j.apcatb.2015.08.037.

[12] M. Meksi, A. Turki, H. Kochkar, L. Bousselmi, C. Guillard, G. Berhault, The role of lanthanum in the enhancement of photocatalytic properties of TiO_2 nanomaterials obtained by calcination of hydrogenotitanate nanotubes, Applied Catalysis B: Environmental, 181 (2016) 651-660.doi:https://doi.org/10.1016/j.apcatb.2015.08.037.

[13] Q. Zhang, Y. Fu, Y. Wu, T. Zuo, Lanthanum-Doped TiO_2 Nanosheet Film with Highly Reactive {001} Facets and Its Enhanced Photocatalytic Activity, European Journal of Inorganic Chemistry, 2016 (2016) 1706-1711.doi:10.1002/ejic.201600006

[14] K. Kočí, I. Troppová, M. Edelmannová, J. Starostka, L. Matějová, J. Lang, M. Reli, H. Drobná, A. Rokicińska, P. Kuśtrowski, L. Čapek, Photocatalytic decomposition of methanol over La/TiO_2 materials, Environmental Science and Pollution Research, 25 (2018) 34818-34825.doi:10.1007/s11356-017-0460-x

[15] K. Azad, P. Gajanan, Photodegradation of methyl orange in aqueous solution by the visible light active Co: La: TiO_2 nanocomposite, Chem Sci J, 164 (2017).doi:10.1007/s10854-019-02619-9.

[16] A. Jraba, Z. Anna, E. Elaloui, Physicochemical properties of La^{3+}-doped TiO_2 monolith prepared by sol–gel approach: application to adsorption and solar photodegradation of ibuprofen, Journal of Materials Science: Materials in Electronics, 31 (2020) 1072-1083.doi:10.1007/s10854-019- 02619-9

[17] Q.C. Wu, Y.F. Zhang, Z. Ji, K. Chen, C.C. Jia, S.W. Yang, Photocatalytic degradation performance of $La^{3+}/Y^{3+}/Eu^{3+}$ co-doped TiO_2 loading on nickel foam, IOP Conference Series: Materials Science and Engineering, 504 (2019) 012036.doi:10.1088/1757-899x/504/1/012036.

[18] T. Yu, X. Tan, P. Chen, H.M. Wang, Lanthanum-Doped Titania Film Coated on Light Leakage Fiber Photo-Degradation Methyl Orange, Advanced Materials Research, 512-515 (2012) 1651-1655.doi:10.4028/www.scientific.net/AMR.512-515.1651.

[19] Z. Jian, Y. Pu, J. Fang, Z. Ye, Microemulsion Synthesis of Nanosized TiO_2 Particles Doping with Rare-Earth and their Photocatalytic Activity, Photochemistry and Photobiology, 86 (2010) 1016-1021.1016-1021. doi:10.1111/j.1751-1097.2010.00773.x.

[20] R. Bao, Y. Yu, H. Chen, W. Wang, J. Xia, H. Li, Effects of Rare Earth Elements and Nitrogen Co-Doped on the Photocatalytic Performance of TiO_2, Crystal Research and Technology, 53 (2018) 1700138.https://doi.org/10.1016/j.micromeso.2009.05.009.

[21] E. Tetteh, S. Rathilal, D. Naidoo, photocatalytic degradation of oily waste and phenol from a local South Africa oil refinery wastewater using response methodology, Scientific Reports, 10 (2020) 1-12.https://doi.org/10.1038/s41598-020-65480-5

[22] M.C. Vebber, J. da Silva Crespo, M. Giovanela, Self-assembled thin films of PAA/PAH/TiO_2 for the photooxidation of ibuprofen. Part I: Optimization of photoactivity using design of experiments and surface response methodology, Chemical Engineering Journal, 360 (2019) 1447-1458.https://doi.org/10.1016/j.cej.2018.10.189.

[23] A. Hafeez, S.A.A. Taqvi, T. Fazal, F. Javed, Z. Khan, U.S. Amjad, A. Bokhari, N. Shehzad, N. Rashid, S. Rehman, Optimization on cleaner intensification of ozone production using Artificial Neural Network and Response Surface Methodology: Parametric and comparative study, Journal of Cleaner Production, 252 (2020) 119833.https://doi.org/10.1016/j.jclepro.2019.119833.

[24] X. Wang, N. Li, J. Li, J. Feng, Z. Ma, Y. Xu, Y. Sun, D. Xu, J. Wang, X. Gao, Fluoride removal from secondary effluent of the graphite industry using electrodialysis: Optimization with response surface methodology, Frontiers of Environmental Science & Engineering, 13 (2019) 51.https://doi.org/10.1007/s11783-019-1132-5

[25] L. Kumaresan, A. Prabhu, M. Palanichamy, E. Arumugam, V. Murugesan, Synthesis and characterization of Zr^{4+}, La^{3+} and Ce^{3+} doped mesoporous TiO_2: Evaluation of their photocatalytic activity, Journal of hazardous materials, 186 (2011) 1183-1192.https://doi.org/10.1016/j.jhazmat.2010.11.124.

[26] S. Mortazavian, A. Saber, D.E. James, Optimization of Photocatalytic Degradation of Acid Blue 113 and Acid Red 88 Textile Dyes in a UV-C/TiO_2 Suspension System: Application of Response Surface Methodology (RSM), Catalysts, 9 (2019) 360.https://doi.org/10.3390/catal9040360.

[27] V.T. Pham, H.-T. T Nguyen, D. Thi Cam Nguyen, H. TN Le, T. Thi Nguyen, N. Thi Hong Le, K.T. Lim, T. Duy Nguyen, T.V. Tran, L.G. Bach, Process Optimization by a Response Surface Methodology for Adsorption of Congo Red Dye onto Exfoliated Graphite-Decorated $MnFe_2O_4$ Nanocomposite: The Pivotal Role of Surface Chemistry, Processes, 7 (2019) 305.https://doi.org/10.3390/pr7050305.

[28] L. Zhao, Q. Li, X. Xu, W. Kong, X. Li, Y. Su, Q. Yue, B. Gao, A novel Enteromorpha based hydrogel optimized with Box–Behnken response surface method: synthesis, characterization and swelling behaviors, Chemical Engineering Journal, 287 (2016) 537-544. https://doi.org/10.1016/j.cej.2015.11.085.

[29] S. Varala, B. Dharanija, B. Satyavathi, V.B. Rao, R. Parthasarathy, New biosorbent based on deoiled karanja seed cake in biosorption studies of Zr (IV): optimization using Box–Behnken method in response surface methodology with desirability approach, Chemical Engineering Journal, 302 (2016) 786-800. https://doi.org/10.1016/j.cej.2016.05.088

[30] B.-y. Tak, B.-s. Tak, Y.-j. Kim, Y.-j. Park, Y.-h. Yoon, G.-h. Min, Optimization of color and COD removal from livestock wastewater by electrocoagulation process: application of Box–Behnken design (BBD), Journal of Industrial and Engineering Chemistry, 28 (2015) 307-315.https://doi.org/10.1016/j.jiec.2015.03.008.

[31] M. Balasubramanian, Application of Box–Behnken design for fabrication of titanium alloy and 304 stainless steel joints with silver interlayer by diffusion bonding, Materials & Design, 77 (2015) 161-169. https://doi.org/10.1016/j.matdes.2015.04.003.

[32] S.C. Ferreira, R. Bruns, H. Ferreira, G. Matos, J. David, G. Brandao, E.P. da Silva, L. Portugal, P. Dos Reis, A. Souza, Box-Behnken design: an alternative for the optimization of analytical methods, Analytica chimica acta, 597 (2007) 179-186.https://doi.org/10.1016/j.aca.2007.07.011.

[33] J. Liu, T. An, G. Li, N. Bao, G. Sheng, J. Fu, Preparation and characterization of highly active mesoporous TiO_2 photocatalysts by hydrothermal synthesis under weak acid conditions, Microporous and Mesoporous Materials, 124 (2009) 197-203.https://doi.org/10.1016/j.micromeso.2009.05.009.

[34] M. Costamagna, L. Ciacci, M.C. Paganini, P. Calza, F. Passarini, Combining the highest degradation efficiency with the lowest environmental impact in zinc oxide based

photocatalytic systems, Journal of Cleaner Production, 252 (2020) 119762.https://doi.org/10.1016/j.jclepro.2019.119762.

[35] E. Özdemir, D. Duranoğlu, Ü. Beker, A.Ö. Avcı, Process optimization for Cr (VI) adsorption onto activated carbons by experimental design, Chemical Engineering Journal, 172 (2011) 207-218.https://doi.org/10.1016/j.cej.2011.05.091

[36] A. Kumar, B. Prasad, I. Mishra, Optimization of process parameters for acrylonitrile removal by a low-cost adsorbent using Box–Behnken design, Journal of Hazardous Materials, 150 (2008) 174-182.https://doi.org/10.1016/j.jhazmat.2007.09.043.

[37] S.T. Akar, F. Sayin, S. Turkyilmaz, T. Akar, Multivariate optimization of the decolorization process by surface modified biomaterial: Box–Behnken design and mechanism analysis, Environmental Science and Pollution Research, 21 (2014) 13055-13068.https://doi.org/10.1007/s11356-014-3245-5.

[38] N. Ameur, G. Ferouani, Z. Belkadi, R. Bachir, J.J. Calvino, A. Hakkoum, A novel approach for the preparation of silver nanoparticles supported on titanate nanotubes and bentonite-application in the synthesis of heterocyclic compound derivatives, Materials Research Express, 6 (2019) 125051.doi:10.1088/2053-1591/ab5734.

[39] G. Ferouani, N. Ameur, R. Bachir, Preparation and characterization of supported bimetallic gold–iron nanoparticles, and its potential for heterogeneous catalysis, Research on Chemical Intermediates, 46 (2020) 1373-1387.doi:10.1088/2053-1591/ab5734.

[40] N. Ameur, R. Bachir, S. Bedrane, A. Choukchou-Braham, A green route to produce adipic acid on TiO_2–Fe_2O_3 nanocomposites, Journal of the Chinese Chemical Society, 64 (2017) 1096-1103.https://doi.org/10.1002/jccs.201700130.

[41] D. Xu, L. Feng, A. Lei, Characterizations of lanthanum trivalent ions/TiO_2 nanopowders catalysis prepared by plasma spray, Journal of Colloid and Interface Science, 329 (2009) 395-403.doi:https://doi.org/10.1016/j.jcis.2008.09.048.

[42] W. Zhang, X. Li, G. Jia, Y. Gao, H. Wang, Z. Cao, C. Li, J. Liu, Preparation, characterization, and photocatalytic activity of boron and lanthanum co-doped TiO_2, Catalysis Communications, 45 (2014) 144-147.doi:https://doi.org/10.1016/j.catcom.2013.11.008.

[43] L.-W. Sun, H.-Q. Shi, W.-N. Li, H.-M. Xiao, S.-Y. Fu, X.-Z. Cao, Z.-X. Li, Lanthanum-doped ZnO quantum dots with greatly enhanced fluorescent quantum yield, Journal of Materials Chemistry, 22 (2012) 8221-8227.doi:10.1039/C2JM00040G

[44] V. Štengl, S. Bakardjieva, N. Murafa, Preparation and photocatalytic activity of rare earth doped TiO_2 nanoparticles, Materials Chemistry and Physics, 114 (2009) 217-226.https://doi.org/10.1016/j.matchemphys.2008.09.025

[45] V.H.-T. Thi, B.-K. Lee, Effective photocatalytic degradation of paracetamol using La-doped ZnO photocatalyst under visible light irradiation, Materials Research Bulletin, 96 (2017) 171-182.http://dx.doi.org/10.1016/j.materresbull.2017.04.028

[46] Z. Fandi, N. Ameur, F.T. Brahimi, S. Bedrane, R. Bachir, Photocatalytic and corrosion inhibitor performances of CeO_2 nanoparticles decorated by noble metals: Au, Ag, Pt, Journal of Environmental Chemical Engineering, (2020) 104346.https://doi.org/10.1016/j.jece.2020.104346

[47] I. Asiltürk, S. Neşeli, Multi response optimisation of CNC turning parameters via Taguchi method-based response surface analysis, Measurement, 45 (2012) 785-794.https://doi.org/10.1016/j.measurement.2011.12.004

[48] K. Yetilmezsoy, S. Demirel, R.J. Vanderbei, Response surface modeling of Pb (II) removal from aqueous solution by Pistacia vera L.: Box–Behnken experimental design, Journal of Hazardous Materials, 171 (2009) 551-562. https://doi.org/10.1016/j.jhazmat.2009.06.035

[49] K. Anupam, S. Dutta, C. Bhattacharjee, S. Datta, Adsorptive removal of chromium (VI) from aqueous solution over powdered activated carbon: Optimisation through response surface methodology, Chemical Engineering Journal, 173 (2011) 135-143.https://doi.org/10.1016/j.cej.2011.07.049

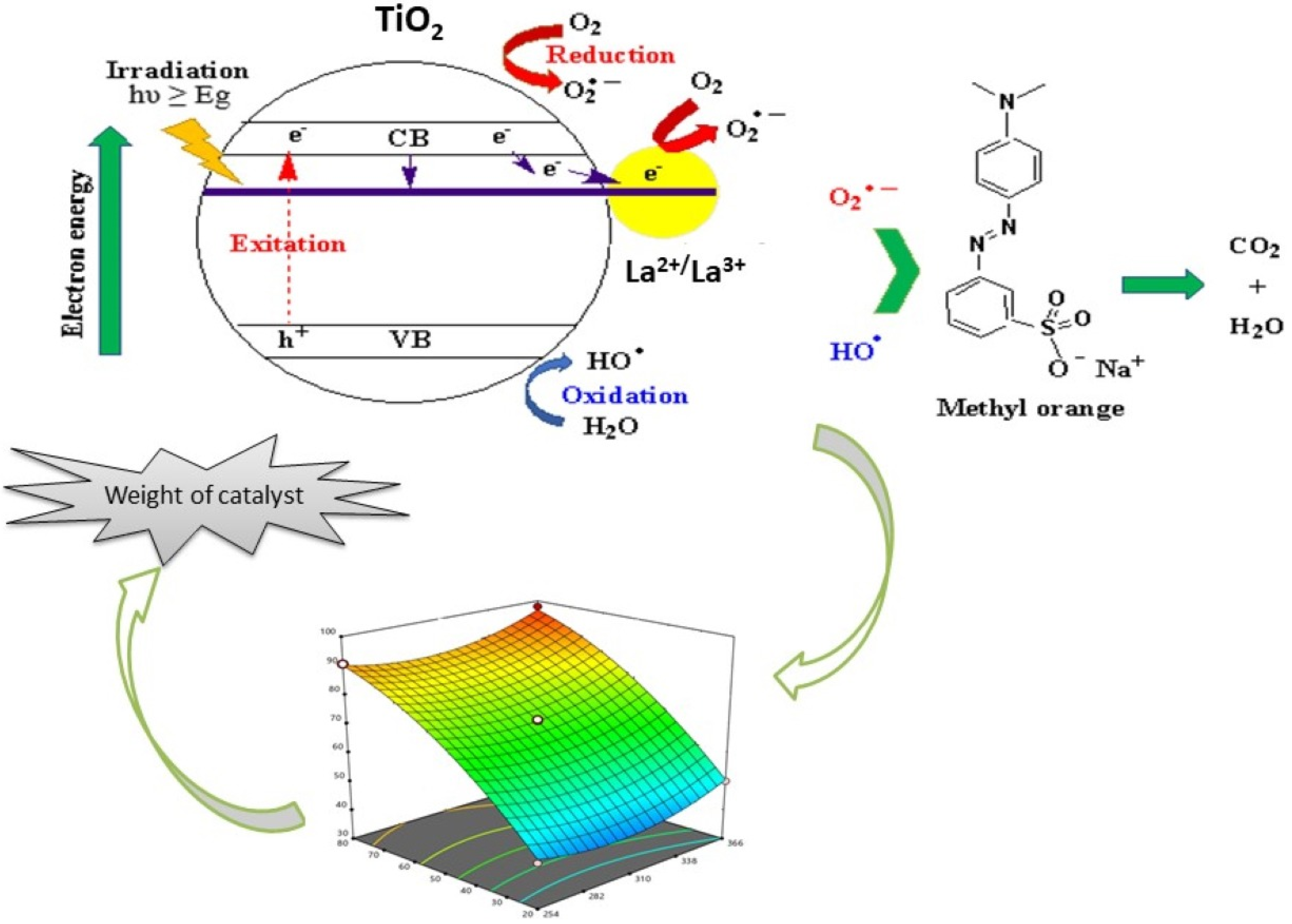
TiO2
O2
Reduction
O2•−
O2
O2•−
Irradiation
hυ ≥ Eg
Electron energy
e-
CB
e-
e-
e-
Exitation
La2+/La3+
h+
VB
HO•
Oxidation
H2O
O2•−
HO•
N
N
N
O
S
O
O−
Na+
Methyl orange
CO2
+
H2O
Weight of catalyst
100
90
80
70
60
50
40
30
80
70
60
50
40
30
20
254
282
310
338
366